Unsteady behavior in forced ow over a backward-facing step

Camila Chovet, Marc Lippert, Laurent Keirsbulck, Jean-Marc Foucaut

Unsteady behavior in forced flow over a backward-facing step

Camila Chovet[a], Marc Lippert[b] and Laurent Keirsbulck[c]
University of Valenciennes and Hainaut-Cambresis, Valenciennes, 59313, France

Jean-Marc Foucaut[d]
Professor, Villeneuve d'Ascq, 59655, France

The unsteady behavior of a turbulent flow over a backward-facing step was investigated under controlled actuation at a $Re_h = 31500$. Initial measurements were made changing the periodic forcing frequency St_a from 0.045 to 0.453. The best forcing frequency was observed at a dimensionless frequency of $St_a = 0.226$ and is associated with the shedding frequency. This frequency can effectively reduce the reattachment length and thus the recirculation area. A further study of the dynamical aspects of the unactuated and actuated flows is also presented. The velocity fields were measured using a particle image velocimetry (PIV) system. POD techniques were used to analyze the flow. With this procedure, the pressure fluctuation power spectra was separated in 5 different modes. The two first modes contained a predominant peak at around 0.12 corresponding to the flapping motion (low frequency of the large scale structures). The other modes (from 3 to 5) showed a transitional and increasing peak that is related to the shedding phenomena. Results suggest that an excitation on the shedding frequency leads to a decrease of the external separation length L_r, an increase of the internal separation length X_r and a further decrease of the recirculation area.

[a] Ph.D. Student, Mechanical Department, LAMIH UMR8201, camila.chovet@etu.univ-valenciennes.fr.
[b] Laboratory Engineer, Mechanical Department, LAMIH UMR8201, Marc.Lippert@univ-valenciennes.fr.
[c] Professor, Department, LAMIH UMR8201, Laurent.Keirsbulck@univ-valenciennes.fr.
[d] Professor, Mechanical Laboratory, LML UMR8107, jean-marc.foucaut@ec-lille.fr.

Nomenclature

A_{r} = Recirculation area [m^2]

AR = Aspect ratio of the backward-facing step

Cp = Mean pressure coefficient

Cp_{rms} = RMS Pressure coefficient

C_{μ} = Dimensionless momentum coefficient

δ = Boundary layer thickness [m]

ER = Expansion ratio of the flow configuration

f = Frequency [Hz]

f_{a} = Actuation frequency [Hz]

h = Height [m]

I_{jet} = Time-average jet momentum

L_{r} = External separation length or recirculation length [m]

p = Fluctuating pressure [Pa]

Re_{δ} = Reynolds number based on the boundary layer thickness [m]

Re_{h} = Reynolds number based on the step height [m]

ρ = Air density [$\mathrm{kg/m}^3$]

S_{jet} = Total outlet cross-section of the micro-jets

S_{ref} = Reference controlled surface of the backward-facing step

St_{a} = Strouhal number based on the step height and actuated frequency

St = Strouhal number based on the un-actuated reciculation length ($\mathrm{L_r}$)

t = Time [s]

T = Period of time [s]

U_0 = Free-stream velocity [m/s]

u_{jet} = Jet velocity [m/s]

V_{jet} = Jet velocity amplitude [m/s]

X_{r} = Internal separation length [m]

x, y, z = Spatial coordinates (origin of the step) [m]

w_{z} = Span-wise fluctuation vorticity [m/s]

I. Introduction

The control of separated and reattaching flows is an essential issue for practical applications and future development of computational techniques to correctly predict them. Despite the simplification associated with the immobility of the point or line of separation, such flows retain a number of fluid-dynamic complexities that must be properly considered [29]. Moreover, these flows give rise to unsteadiness, pressure fluctuations, structure vibrations and noise [9]. Flow control over separated and reattaching flows can be classified into two groups: passive and active control. Passive control has been widely applied, however, is restricted by design and practical considerations and cannot be 'turned off' when not needed. Due to the constraints presented in this strategy, studies on active flow control has rapidly developed. Some advantages of active flow control are: imitation of passive control, ability to turn on or off depending on the requirement. Furthermore, active control can be combined with passive deflected surfaces to improve actuation [2, 13, 32].

Cattafesta and Shelpak [4] give an extensive overview of possible actuation mechanisms. Active control is initially performed in an open-loop manner (i.e., pre-determined and independent of the flow state). To control the reattachment of the separated flow, two main approaches raise from past investigations. Continuous suction or injection to shear layer has been applied to various types of flow configurations [1, 30, 37]. Periodically perturbing the shear layer on the separation trailing edges, using synthetic or pulsed jet actuators, was found to be an effective tool to control these flows [11, 16, 21, 28, 38]. Previous studies showed that a periodic perturbation exhibited better reattachment control than continuous perturbation [27, 33]. A common result obtained from periodic perturbation is that the reattachment length behind the step is remarkably reduced when the frequency of the imposed perturbation falls in a certain range. Bhattacharjee et al. [3] claimed that the most effective non-dimensional forcing frequency, so called Strouhal Number, was between 0.2 and 0.4.

Among reattaching, separated flows, the two-dimensional, backward-facing step flow is the simplest configuration; nevertheless, it includes all the significant features. In this paper we report an experimental investigation of a backward-facing step flow, at $\mathrm{Re_h} = 31500$, manipulated by time-periodic forcing close to the step edge. An initial modification of the mean external and internal

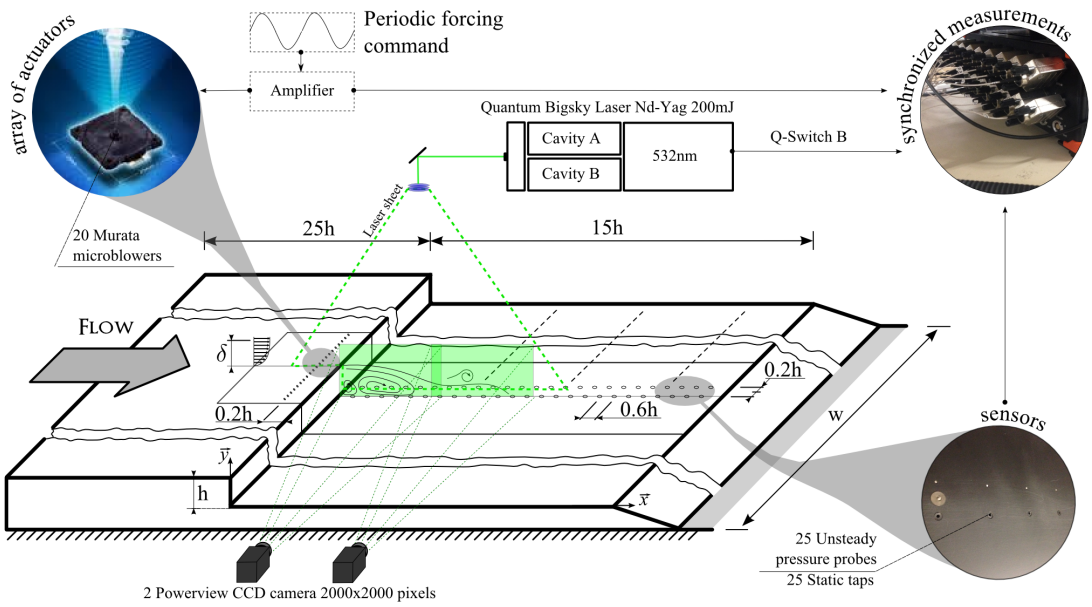

Fig. 1 Backward facing step sketch

separation lengths is done for a periodic forcing frequency St_a from 0.045 to 0.453. The results obtained were compared with previous investigations. A further study of the dynamical processes on the actuated flow, which lead to the reduction of the re-attachment zone, will be done using proper orthogonal decomposition approach.

II. Experimental apparatus

A. Facility and backward facing step model

The experiments were performed in an optically accessible closed-loop wind tunnel of the Mechanical Department at LAMIH. The test section had a square cross-section of 2m × 2m with the length being 10m. The top and side-walls of the test section were made of plexiglass to allow flow visualizations. The velocity range in the section is 0.5 to 60m/s. The free stream flow velocity was measured by a Pitot tube in the inlet after the ramp. The step height h of the backward-facing step was 83mm, resulting in expansion ratio ER of 1.04. The aspect ratio AR based on h and channel span was 24, assuring an effectively nominally two-dimensional flow [10]. A 3D scheme of the test set-up was given in figure 1. The origin of the co-ordinate system was located at the edge of the step. The x-axis represents the stream wise flow direction, the y-axis the normal direction to the

flow and the z-axis the spanwise or cross-stream flow. Measurements have been performed at free stream velocity of $U_0 = 5.5$m/s, $Re_h = 30450$ ($\delta = 0.75$h, $Re_\delta = 22825$).

B. The perturbation technique

The flow perturbation was introduced through a row of actuators composed of Murata micro-blowers. The row was placed on the span wise center of the test section, with a length of 20% test section width. This free space, from the actuation area to the walls, prevents flow interactions between the backward-facing step and the wall corners. The actuators were mounted upstream the separation edge at a distance of 0.2h, as shown in figure 1. This location was chosen following previous configurations [15].

The air actuation system was composed of 20 Murata micro-blowers, which use piezoelectric devices, and distribute the air flow through micro-nozzles. The distance between the two neighboring micro-blower nozzles was 20 mm. The micro-jets axes were perpendicular to the step wall. Contrarily to others classical pulsed jets devices, Murata micro-blowers do not need external pressure source to produce the pulsed jet, only a power supply of 5 to 20 Volts is needed to drive them. They were also able to provide, without significant overshoot, any kind of velocity time-history profiles. Murata micro-blowers can produce a wide range of signals, not only square- or sine- like signals of the classical devices [6]. These actuators are really interesting for the closed-loops flow control applications. The mean jet velocity, u_{jet} is proportional to the voltage command till to 100Hz and each micro-blower can provide a mean velocity between 0 m/s to 30 m/s.

The perturbation was design to follow the expression:

$$u_{jet}(t) = V_{jet}\sin(2\pi.f_a.t), \tag{1}$$

were V_{jet} is the velocity actuation amplitude, set constant to 25m/s (correspond to 20V), and f_a the frequency of the perturbation. The pulsed micro-blowers was quantified using the dimensionless momentum coefficient, C_μ:

$$C_\mu = \frac{< I_{jet} >}{1/2.\rho.U_0^2.S_{ref}}, \qquad < I_{jet} > = \rho.S_j.\frac{1}{T}\int_0^T u_{jet}^2 dt = \rho.S_{jet}.< u_{jet}^2 > \tag{2}$$

where $< I_{jet} >$ is the time-average jet momentum, S_{jet} is the total outlet cross-section of the micro-jets, S_{ref} is the reference controlled surface of the backward-facing step equal to (5h) × h. For the forcing frequency flow control, two other parameters, named the dimensionless frequency or Strouhal number, were used for the characterization of the actuation efficiency, they were define as:

$$St_a = \frac{f_a.h}{U_0} \tag{3}$$

and

$$St = \frac{f_a.L_{r0}}{U_0}, \tag{4}$$

where L_{r0} is the external separation length, commonly known as the recirculation point, of the un-actuated flow.

C. Time resolved surface pressure- and velocity- measurements

Wall static pressures were measured with 25 static pressure taps distributed downstream of the back-facing step in the stream wise direction. These taps were located at a distance of 0.2h from the middle of test section in the spanwise direction, see figure 1. The first tap was located 25mm from the step edge and the distance between two consecutive taps was 50mm (x/h = 0.6), giving a pressure measure zone of 14.75h. Unsteady pressure measurements were also taken from 25 sub-miniature piezo-resistive Kulite XCQ-062 sensors, with a nominal measurement range of 35 kPa. Flush-mounted Kulite transducers were placed at the same x location as the static ones but in the middle of the test section.

D. PIV arrangement and synchronization procedure

A standard two-component TSI particle image velocimetry (PIV) system was employed for flow-field measurements. Oil particles with 1μ diameter, generated with a jet atomizer upstream of the stagnation chamber, were seeded in the channel. This location allows homogenous dispersion

of the particles throughout the test section. The tracer particles were illuminated by a double-pulse laser system generating the light sheet. The frequency-doubled laser (Q-switched Nd:YAG operating at 532 nm; dual-head BigSky) emits laser pulses with a maximum energy of 200 mJ. Images of the tracers were recorded from the direction normal to the light sheet using two cameras (2000×2000 pixels charge-coupled-device Powerview with a 50 mm optical lens) with a camera resolution of 19.2 px/mm. The number of double-frame pictures recorded for each experience was 2000 assuring velocity field statistics convergence. The dynamic range was approximately 30 px and the interrogation window size is 16×16 pixels with an overlap of 50%. The PIV time-uncorrelated snapshots were recorded with a repetition rate of a 7 Hz. The measurement area was approximately $7.3h \times 1.8h$ on the x-y plane passing through center of the backward facing step.

Dynamic pressure measurements were recorded simultaneously with the PIV measurements. To achieve the synchronization, a 32-channel A/D converter Dewesoft data acquisition system was used to simultaneously record the Q-switch signal of the second laser and the pressure transducer signals. The data acquisition system used a sampling frequency of 10kHz, and a cutoff filtered at 3kHz. In the flow control case, the actuation signal was also recorded.

III. Results

A. Base flow

The main characteristics of the un-actuated base flow were investigated and constitute the reference case for the subsequent actuated flow case. The mean spanwise vorticity field was shown in figure 2(a), associated streamlines were also included in the figure to highlight the mean flow structure. A classical backward-facing step flow topology. The boundary layer appears as a concentrated region of negative vorticity that detaches from the step edge, growing in width in the streamwise direction, to finally reattach at an external separation length (L_r) downstream of the step. Beneath the shear layer, two recirculation regions were seen. The first one was a clockwise recirculation zone that stretches from an internal separation length of $X_r = 0.83$ to an external separation length of $L_r = 5.59$, the latter will be further modify by the actuation. Near the step, within the $X_r = 0.83$ region, the streamlines showed the secondary recirculation zone. Previous studies [19, 22, 31] were also able to see this secondary recirculation bubble.

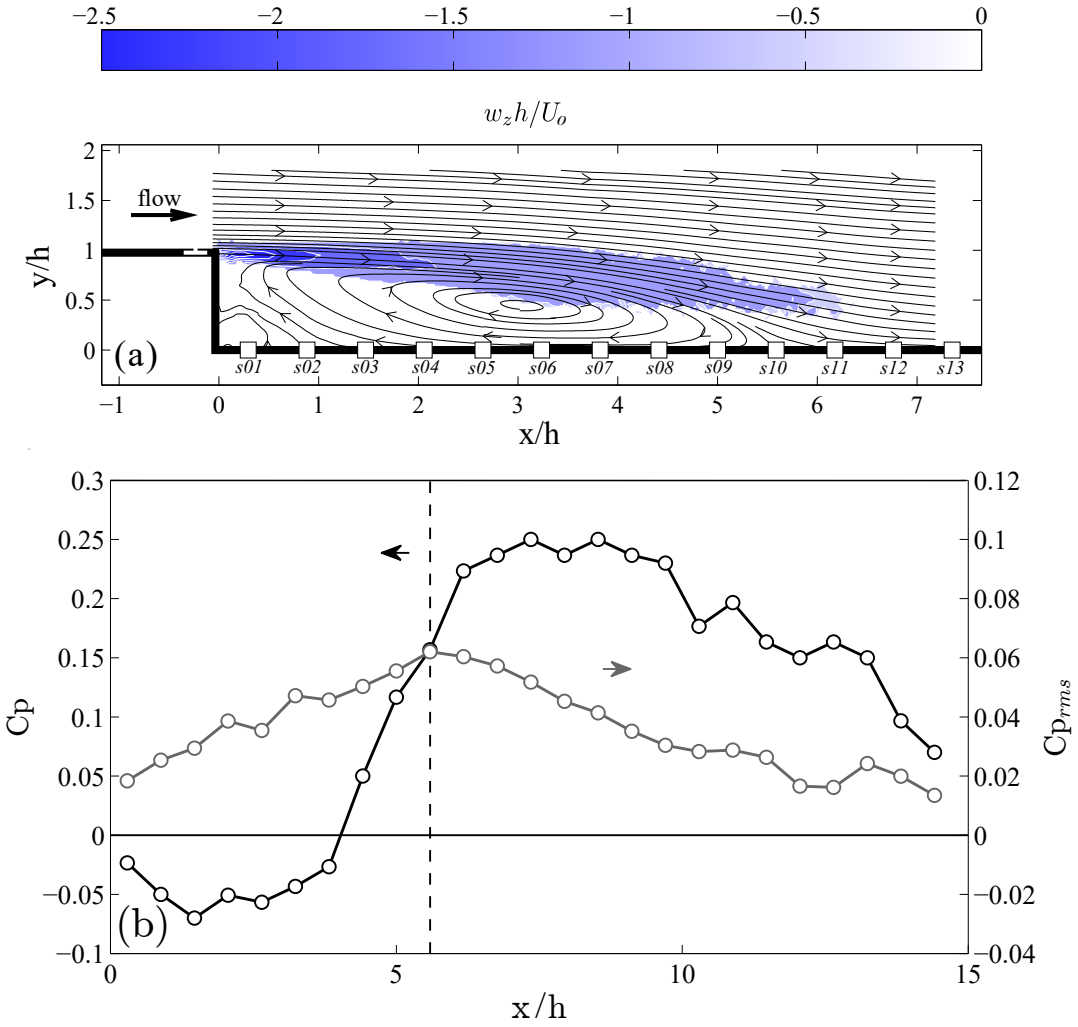

Fig. 2 (a) Contour map of the mean spanwise vorticity field with associated streamlines, (b) Mean- and rms-pressure distributions. Dash-line marking the L_r value.

The mean- and the rms-pressure streamwise distributions downstream of backward-facing step ares shown in figure 2(b). The mean-pressure coefficient, $Cp = (p - p_{ref})/(1/2\rho U_0^2)$ was plotted along the ordinate as a function of the streamwise coordinate (x/h). Note that p is the pressure measured along the surface of the model and p_{ref} is a reference pressure measured with a static-pressure tap located at x/h = 30. A large region of low-pressure level was seen and zero-crossing section of Cp was located in the neighborhood of x/h ≈ 4. A rapid increase of Cp was displayed, i.e. the beginning of the pressure recovery area moves rapidly upstream. The maximum Cp peak was reached at the vicinity of where the flow reattaches, as described by [14]. Immediately after separation, the pressure gradient becomes adverse as the flow expands. This mean-pressure distribution shows a classical,

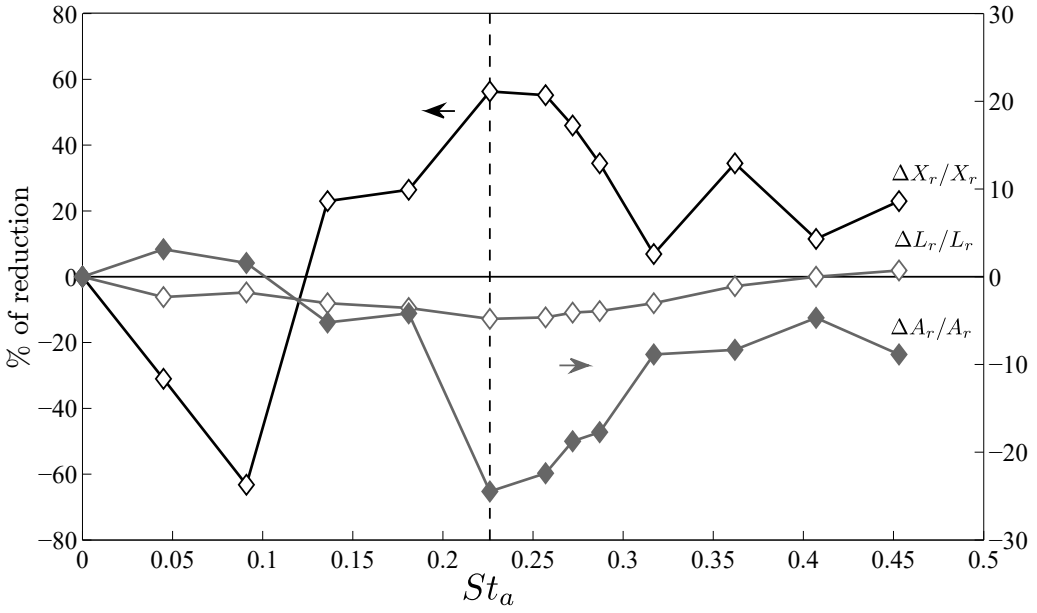

Fig. 3 Reattachment lengths X_r, $L_r$and recirculation area A_r as a function of the Strouhal number St_a. Dashed line denotes the optimal actuation frequency.

backward-facing step, pressure profile and is consistent with previous findings [5, 8, 14, 17, 19].

The rms pressure measurements, $Cp_{rms} = p_{rms}/(1/2\rho U_\infty^2)$ was also plotted in figure 2(b) as a function of x/h. The level of fluctuating pressure rises in the downstream direction reaching a maximum value close to the reattachment point L_r. The shape of the rms distribution is consistent with previous results documented in the literature for a backward-facing step [12, 18, 23].

B. Forcing frequency flow control

Among the various parameters characterizing the backward-facing step flow, the reattachment length L_r is frequently used as a representative quantity in a time-mean sense. However, other important parameters, normally not taken into account in previous investigations, are the mean secondary separation location X_r and the recirculation A_r. To obtain the former lengths, Simpsons *et al.* [34] estimated the points where the backward flow probability (BFP) reached a value of 50%. The internal and external lengths were estimated from the BFP field at the vicinity of the wall (y/h = 0.07) and further shown in figure 6. The recirculation areas were also obtained from the BFP fields lower than 50% (blue zone in figure 6) .

To actively control the flow, experiments were carried out varying the frequency (f_a) of the

f_a (Hz)	St_a	X_r/h	L_r/h	A_r (m^2)	$\Delta X_r/X_r$ (%)	$\Delta L_r/L_r$ (%)	$\Delta A_r/A_r$ (%)
0	0.000	0.87	5.62	0.0192	0.00	0.00	0.00
3	0.045	0.60	5.49	0.0198	-31.03	-2.31	3.13
6	0.091	0.32	5.52	0.0195	-63.22	-1.78	1.56
9	0.136	1.07	5.45	0.0182	22.99	-3.02	-5.21
12	0.181	1.10	5.42	0.0184	26.44	-3.56	-4.17
15	0.226	1.36	5.35	0.0145	56.32	-4.80	-24.48
18	0.272	1.27	5.39	0.0156	45.98	-4.09	-18.75
21	0.317	0.93	5.45	0.0175	6.90	-3.02	-8.85
24	0.362	1.17	5.56	0.0176	34.48	-1.07	-8.33
27	0.407	0.97	5.62	0.0183	11.49	0.00	-4.69
30	0.453	1.07	5.66	0.0175	22.99	0.71	-8.85

Table 1 Reduction of the recirculation lengths/area by periodic forcing frequency flow control

periodic actuation command (Eq. (1)). The local forcing frequency was changed in the range of $0.045 \leq St_a \leq 0.453$. Both internal and external separation points and the separation area, as a function of the Strouhal Number, were shown in figure 3. All values were normalized by those of the un-actuated experiment. The external reattachment length and the recirculation area first decrease with increasing St_a before they reach a minimum at $St_a = 0.226$ and then increase again, this behavior was stronger for A_r. On the contrary, the internal separation point increases and decreases reaching a peak at the same actuated frequency $St_a = 0.226$, denoted with dashed line. The optimal forcing frequency was observed at $St_a = 0.226$, $f_a = 15$Hz, and could be associated with the shedding phenomena. For this frequency, X_r increases up to 38.4% while L_r and A_r decrease 4.8% and 19.0%, respectively (see table 1). This optimal forcing is consistent with those obtained in previous experiments [3, 8, 23, 36, 37]. Results from all the actuated cases studied were shown in table 1 and corroborate the effectiveness of pulsing jet injection with forcing frequency to reduce the separation length [26].

Spectral analysis may be used to shed light on why a particular perturbation frequency leads to a preferential response of the perturbed baseline flow. figure 4 shows a log-log plot of the pressure

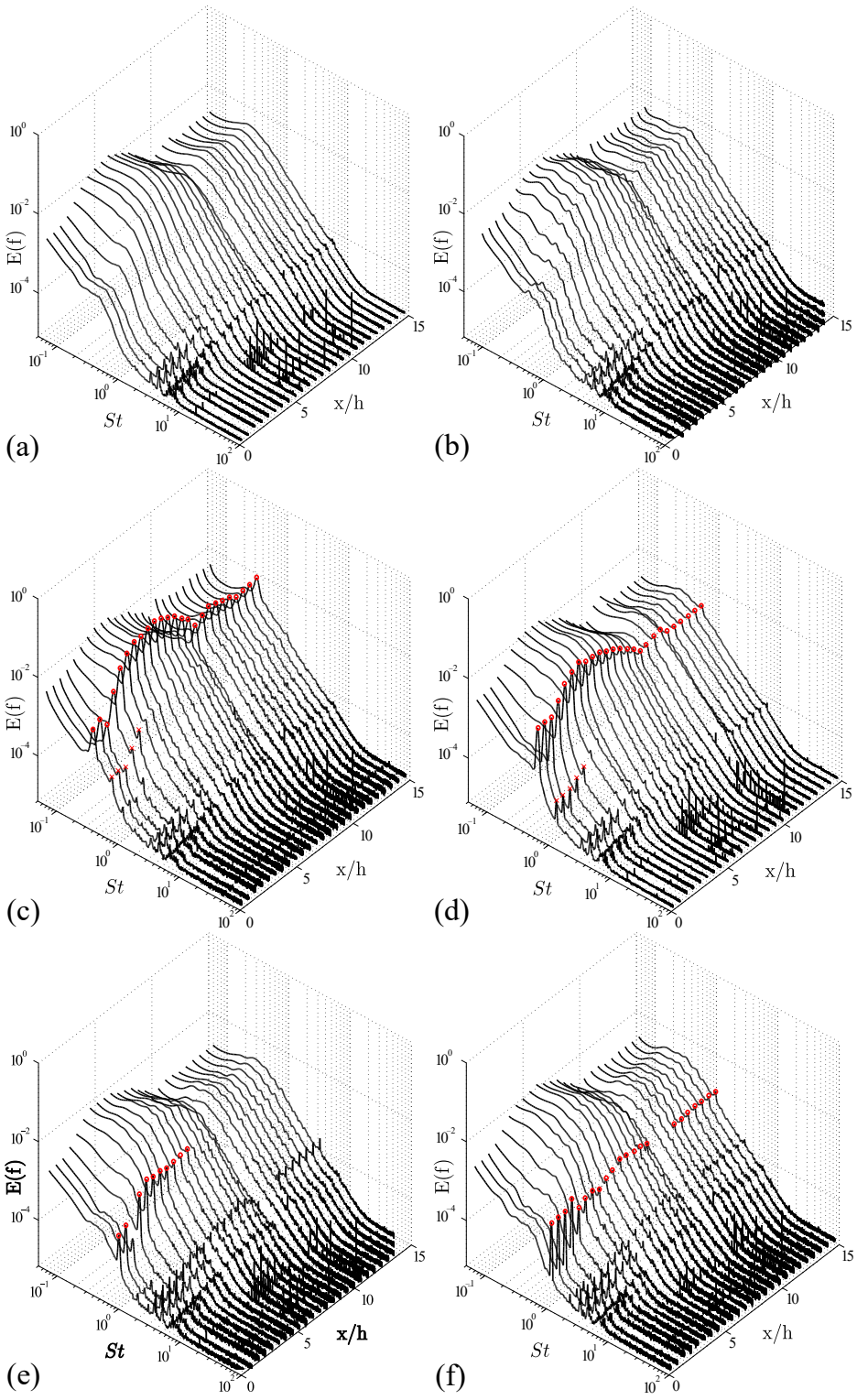

Fig. 4 Power spectra of wall-pressure fluctuations for different x/h locations at $\mathrm{Re_h} = 30450$ **for: (a)Un-forced; (b)**$\mathrm{Sta} = 0.045$**; (c)**$\mathrm{Sta} = 0.136$**; (d)**$\mathrm{Sta} = 0.226$**; (e)**$\mathrm{Sta} = 0.317$**; (f)**$\mathrm{Sta} = 0.407$**.**

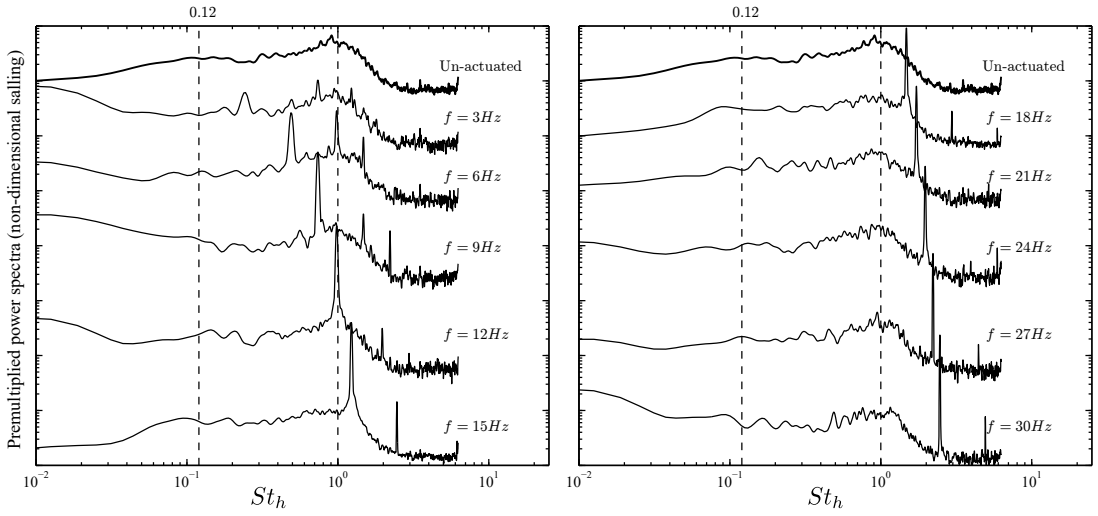

Fig. 5 Non-dimensional premultiplied power spectra of fluctuating wall pressure measured at x/h = 1.5 for un-forced and forced flows.

fluctuations spectra at several x/h locations downstream the step for un-actuated and actuated flows. For all the cases the dynamical behaviors change as a function of the probe position. Four different regions can be identified. The first region, situated from step edge up to x/h ≈ 1.5, shows a low pressure fluctuation where the spectra are dominated by both low- and high-frequencies. A second region, with a transition that occurs from x/h ≈ 1.5, to a merged frequency value, at x/h ≈ 4.5. The third one, corresponding to the recirculation region from x/h = 4.5 to 6.5, where the pressure fluctuations are strong and high energy levels, were clearly visible. The last region represents the reattached zone where the behavior approaches a typical turbulent boundary layer spectrum. This global mechanism is also reported for the same configuration by Spazzini *et al.* [35]. For the actuated cases, the forcing frequency peaks were also seen and marked with a red circle ($St_h = St_a$). The actuation peaks appear in the power spectra after $St_a > 0.045$, and strongly increase in size as St_a increases. Also after the same Strouhal number, the peak depth in the in the x/h direction, e.g., points where the pressure probes sensed the actuation command, was seen. Close to the optimal case the actuation frequency can be sens by all the pressure probes, suggesting that these frequencies can perturbed the flow in a greater degree. Once the Strouhal number reaches its optimal value, the size and depth of the actuation peaks decreases.

To better understand the flow response to different actuation the non-dimensional pre-multiplied

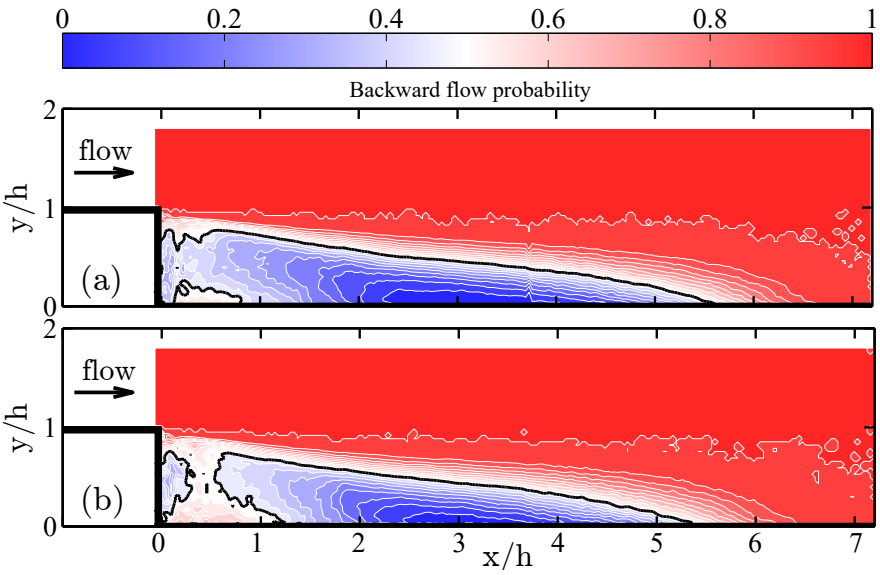

Fig. 6 Backward flow probability field for (a) Un-actuated; (b) actuated at $St_a = 0.226$. Solid line denotes the 50% value of the BFP

power spectra of fluctuating wall pressure measured at $x/h = 1.5$ was presented in figure 5 for both un-forced and forced cases. From results, two frequency peaks can be observed. The first one $St = 0.12$ corresponds to a classical well-defined flapping frequency and a broad band one at around $St = 1$ related to the shedding frequency of the shear-layer structures. These peaks agree well with those obtained in previous investigations [23]. When the flow was forced at $St_a = 0.226$, a strong peak emerged in the spectra at this frequency. The magnitudes of this peak was much larger than the peak without forcing. Also, sub-harmonic frequencies were observed for certain cases, see $St_a = 0.136$, but were polluted with noise.

Hereafter, the optimal frequency will be used to study the behavior of the perturbed flow. PIV measurements were performed for the un-actuated and actuated cases, the backward flow probability (BFP) fields obtained were shown in figure 6(a) and figure 6(b), respectively. From the figures the strong reduction of the recirculation area (blue region) was clearly seen , specially close to the step ($x/h \leq 1$). This reduction at the vicinity of the step creates a positive velocity injection which interacts with the shear-layer vortexes generated at the step edge.

The BFP values extracted at the vicinity of the wall ($y/h = 0.07$) were plotted in figure 7 for the unforced flow (black line) and periodic forcing actuation (red line). The increase of the internal

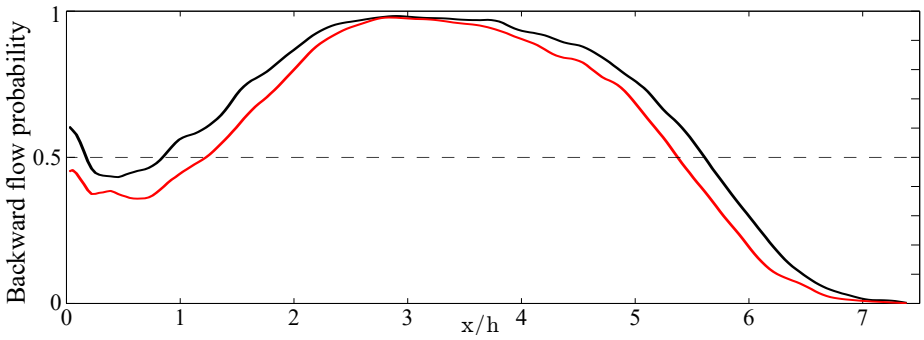

Fig. 7 Profiles of the backward-flow probability at y/h=0.07 for: un-actuated case (black line) and actuated at $\mathrm{St_a} = 0.226$ case (red line)

separation length and the decrease of the external separation point were clearly, corroborating once more the ability of periodic forcing actuation to control the flow.

C. Control mechanisms induced by the forcing frequency control using POD

In order to filter the different components involved in the flow dynamics, time-resolved velocity fields measured with PIV were decomposed using proper orthogonal decomposition (POD) technique. Lumley [24] proposed the proper orthogonal decomposition as an unbiased technique for studying coherent structures in turbulent flows. POD is a logical way to build basis functions that capture the most energetic features of the flow. The POD snapshot method used in the present study is detailed by Chovet *et al.* [7]. This decomposition results in spatial modes representatives of energetic events and each mode represents the contribution of the total turbulent energy of the flow field. Figure 8(a) shows the cumulative energy of the first fifteen velocity modes for un-actuated (black bars) and actuated (red bars) flows. For both cases, The energy fraction of the first and the second POD modes were found to contain almost 20% of the total flow energy, and the first fifteen modes comprise 50% of the total turbulent energy. When the actuation was turned on, the cumulative energy increased. Hereafter, only the 5 first modes will be analyzed; the experimental modes above the fifth were contaminated by noise [25].

To further examine the relation between the motions and wall-pressure fluctuation in the frequency domain, the QSE-POD complementary techniques was used [7]. The non-dimensional pre-

multiplied power spectra of the estimated QSE-POD temporal coefficients for mode 1 to 5 were plotted in Fig. 8(b). From the two first modes, a dominant peak at $f.L_r/U_0 = 0.12$ was clearly seen and corresponds to the flapping frequency. The other modes highlight a transitioning and increasing peak associated to the shedding frequency. When actuation was applied, a peak around $f.L_r/U_0 \approx 1$ was clearly visible. This peak strongly modifies the transitioning peak of the shedding phenomena, specially for the mode 5 where the transitioning shedding peak coincides with the actuation peak. It is also possible to conclude that the 3^{rd}, 4^{th} and 5^{th} mode could be retained if the interest is focused in the shedding process. Results suggest that a modification in the shedding frequency leads to a decrease of L_r, an increase of X_r and a further decrease of the recirculation area.

Figure 9 shows the low-order POD velocity modes n = 1 to 5, with corresponding vorticity modes, for the un-forced flow figure 9(a-e) and the actuated $St_a = 0.226$ figure 9(f-j). The POD basis functions are non-dimensional and the vorticity calculated from the POD mode ω_z was normalized with the step height h. These modes represent the most common events being developed in the fluctuating velocity/vorticity fields. Typical patterns in the POD spatial modes were clearly seen. For both cases, the two first modes present elongated vorticity regions. A round and regular shape in the streamwise direction was clearly seen for the other modes. However, the actuated case showed smaller uniformly shaped vortical structures (either positive or negative), specially for the 5^{th} mode. The result obtained in the mode 5 corroborates the concurrence between the actuation frequency and the shedding peak. This relatively small degree of elongation puts in evidence a strong organization of vortical structures in space [22].

D. Conditional approach

Finally, to go further with this dynamical analysis, a conditional approach has to be considered on the entire period of the control flow signal. This method permits to identify the key mechanism inducing the flow control. In the present case, the global flow distribution over the whole domain was not significantly affected by the actuation as shown in Section , however, the actuator produces a periodic inflow and increase the roll-up of the natural Kelvin-Helmholtz oscillation leading to a noticeable reduction of the separated area. This mechanism was highlighted in figure 11 showing the conditional averaging of the velocity field along the period T of the best forcing actuation.

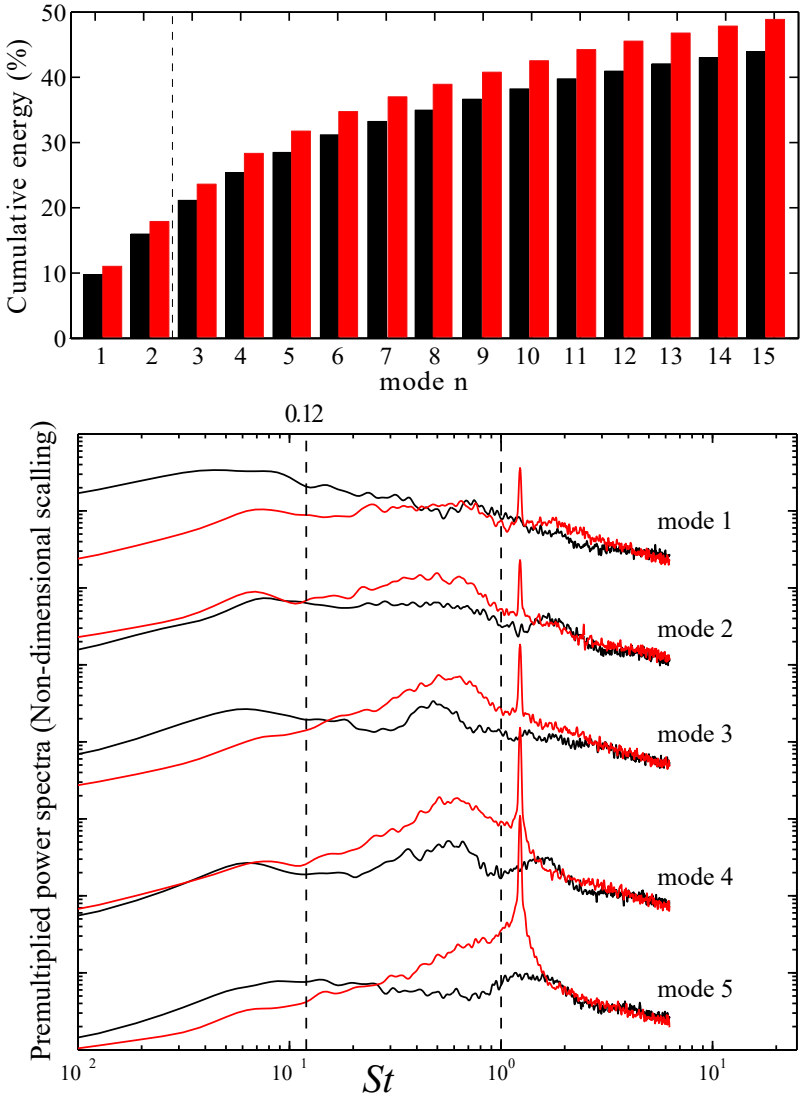

Fig. 8 (a) Cumulative energy from the POD of the velocity fields for: un-actuated case (black bars) and actuated at $St_a = 0.226$ case (red bars). (b) Non-dimensional premultiplied power spectra of the estimated QSE-POD temporal coefficients for mode 1 to 5 of the fluctuating wall pressure measured at $x/h = 1.5$ for: un-actuated case (black lines) and actuated case at $St_a = 0.226$ (red lines)

Figure 10 shows the phase averaged jet velocity profile along the period T for the best case, square symbols represent the moment when the velocity field, obtained from the QSE, was captured. It's important to remark the time delay between the turn on of the actuation and the jet flow interaction with the shear layer. The beginning of the actuation inflow was visible on figure 11(e), where the vortices were clearly perturbed due to the Kelvin-Helmholtz and shedding frequency modification.

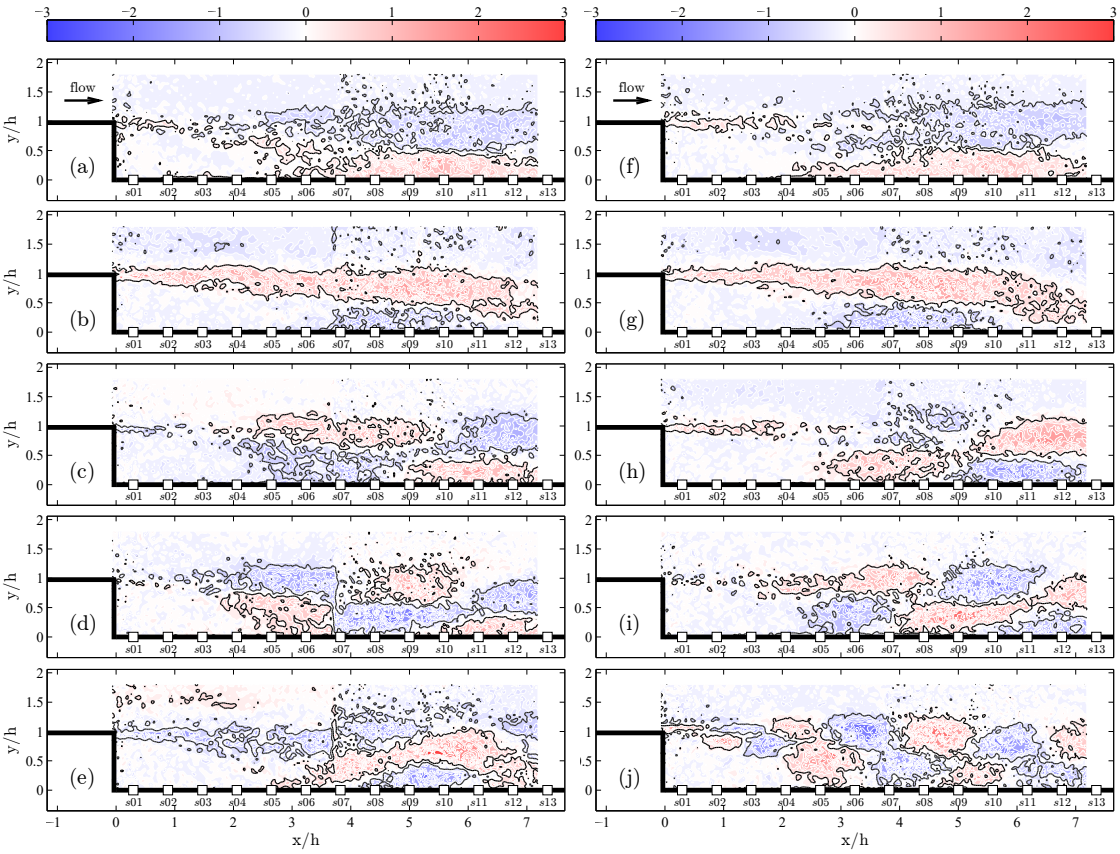

Fig. 9 Low-order POD velocity modes: (a-e) mode 1 to 5 for un-actuated case, (f-j) mode 1 to 5 for actuated case at $St_a = 0.226$. Contour map shows vorticity calculated from the corresponding POD velocity basis function and normalized with the step height, $\omega_z.h$. Vorticity levels between -0.5 and 0.5 were set at zero in order to minimize noise in the contour plots and enhance the visibility of the dominant feature of the modes.

Figure 11(f) to figure 11(k) show the mechanism of "forcing roll-up" induced by the periodic actuation. Also, it was possible to see from the sequence the recur of the flow once the actuation was 'off', see flow similarities in figure 11(j) and figure 11(a).

IV. Conclusion

Experimental flow control in a separated shear layer of a backward-facing step using micro-pulsed jets was done. The control target was to modify key turbulent flow parameters such as: internal separation point, external separation point and recirculation area, more specifically increase the first parameter and reduce the others. Periodic forcing was used to control the flow. Periodic

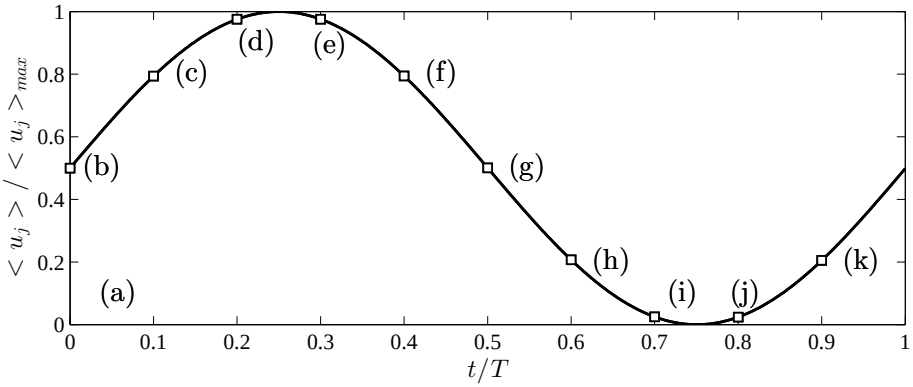

Fig. 10 Phase averaged jet velocity profile along the period T for the best forced case.

forcing was able to significantly decrease the external separation point and the recirculation area, and to move up the internal separation point. From the power spectra wall-pressure fluctuations (at different x/h locations), actuation peaks were clearly obtained after $St_a > 0.045$. The x/h depth of these peaks, e.g., points where the pressure probes sensed the actuation command, was maximum close to the optimal actuation frequency, suggesting that frequencies close to this value can perturbed the flow more thoroughly. The resulting flows were investigated using a PIV system. Furthermore, a study of the dynamical aspects of the un-actuated and actuated flows was also presented. A reconstruction of the flow was done using POD techniques. With this procedure, the pressure fluctuation power spectra was separated in different modes. The two first modes contained a predominant peak at 0.12 corresponding to the flapping motion (low frequency of the large scale structures). The other modes (from 3 to 5) showed a transitional and increasing peak that was related to the shedding phenomena. When actuation was applied, a peak at $f.L_r/U_0 \approx 1$ was clearly visible. This peak strongly modifies the transition peak of the shedding phenomena. Suggesting that a modification in the shedding frequency leads to a decrease of L_r, an increase of X_r and a further decrease of the recirculation area.

Acknowledgments

This work was carried out within the framework of the CNRS Research Federation on Ground Transports and Mobility, in articulation with the ELSAT2020 project supported by the European Community, the French Ministry of Higher Education and Research, the Hauts de France Regional

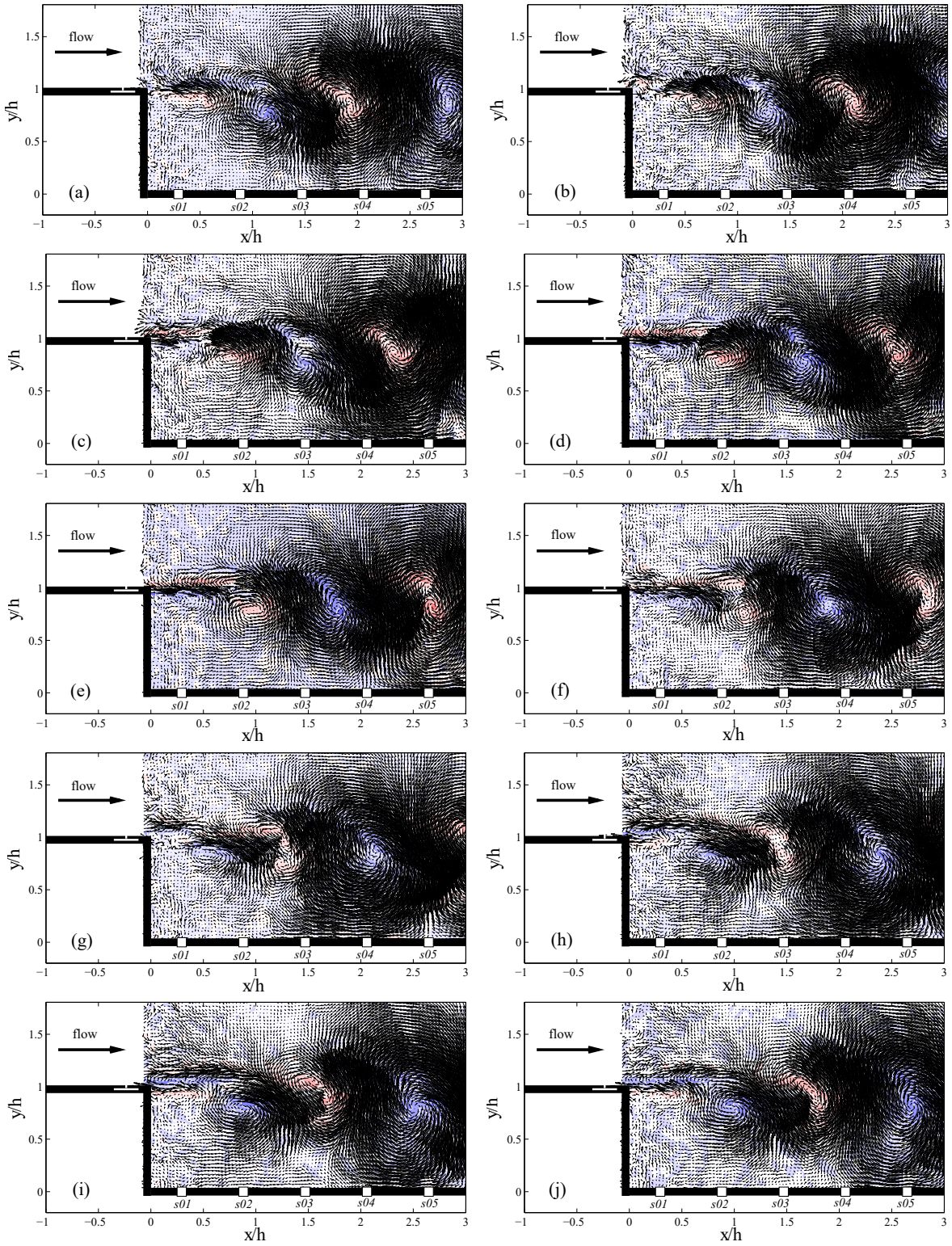

Fig. 11 (b) to (k) Conditional averaging of the velocity fields from the QSE for the 10 phases reported in figure 10.

Council. The authors gratefully acknowledge the support of these institutions.

References

[1] Aubrun, S., McNally, J., Alvi, F., Kourta, A., *Separation flow control on a generic ground vehicle using steady microjet arrays.*, Exp Fluids **51** (5), 1177–1187, 2011.

[2] Barros, D., Boree, J., Noack, B. R., Spohn, A., Ruiz, T., *Bluff body drag manipulation using pulsed jets and Coanda eeffect*, J. Fluid Mech. **805**, 422–459, 2016.

[3] Bhattacharjee, S., Scheelke, B. and Troutt, T.R., *Modification of vortex interactions in a reattaching separated flow*, AIAA Journal **24**, 623–629, 1986.

[4] Cattafesta, L.N. and Sheplak, M., *Actuators for active flow control*, Annual Review of Fluid Mechanics **43**, 247–272, 2011.

[5] Castro, P., Haque, A., *The structure of a turbulent shear layer bounding a separation region*, J. Fluid Mech. **179**, 439, 1987.

[6] Chovet, C., Lippert, M., Keirsbulck, L. and Foucaut, J.-M., *Dynamic characterization of piezoelectric microblowers for separation flow control.*, Sensors and actuators: A Physical **249**, 122–130, 2016.

[7] Chovet, C., Lippert, M., Keirsbulck, L. and Foucaut, J.-M., *Dynamical aspects of a backward-facing step flow at large Reynolds numbers.*, Exp. Fluids(Under revision).

[8] Chun, K.B., Sung, H.J., *Control of turbulent separated flow over a backward-facing step*, Exp. Fluids **21**, 417–426, 1996.

[9] Chun, K.B., Sung, H.J., *Visualization of a locally-forced separated flow over a backward-facing step'*, Exp. Fluids **25**, 133–142, 1998.

[10] De Brederode, V., Bradshaw, P., *Influence of the side walls on the turbulent centerplane boundary-layer in a squareduct*, Trans. ASME I: J. Fluids Eng. **100**, 91–96, 1978.

[11] Dejoan, A., Leschziner, M.A., *Large eddy simulation of periodically perturbed separated flow over a backward-facing step*, International Journal of Heat and Fluid Flow **25**, 581–592, 2004.

[12] Driver, D.M., Seegmiller, H.L., Marvin, J.G., *Time-Dependent Behavior of a Reattaching Shear Layer.*, AIAA Journal **25**, 914–919, 1987.

[13] Englar, R. J., *Advanced aerodynamic devices to improve the performance, economics, handling and safety of heavy vehicles.*,Tech. Rep. SAE Technical Paper 2001–01–2072, 2001.

[14] Farabee, M., Casarella, M.J., *Measurements of fluctuating wall pressure for separated/reattached boundary layer flows*, ASME J. Vib., Acoust., Stress, Reliab. Des. **108**, 301, 1986.

[15] Gautier, N., Aider, J.-L., Duriez, T., Noack, B.R., Segond, M., Abel, M., *Closed-loop separation control using machine learning*, J. Fluid Mech. **770**, 442–457, 2015.

[16] Glezer, A., Amitay, M., Honohan, A.M., *Aspects of low-and high-frequency actuation for aerodynamic flow control.*, AIAA Journal **43** (7), 1501–1511, 2005.

[17] Hasan, M.A.Z., *The flow over a backward-facing step under controlled perturbation : laminar separation*, J. Fluid Mech. **238**, 73–96, 1992.

[18] Heenan A.F., Morrison J.F. *Passive control of pressure fluctuations generated by separated flow*, AIAA Journal **36**, 1014–1022, 1998.

[19] Hudy, L.M., Naguib, A., Humphreys, W.M., *Stochastic estimation of a separated-flow field using wall-pressure-array measurements*, Phy. of Fluids **19**, 024103, 2007.

[20] Hung, L., Parviz, M., John, K., *Direct numerical simulation of turbulent flow over a backward-facing step*, J. Fluid Mech. **330**, 349–374, 1997.

[21] Joseph, P., Amandolese, X., Edouard, C., Aider, J-L., *Flow control using MEMS pulsed micro-jets on the Ahmed body.*, Exp Fluids **54** (1), 1–12, 2013.

[22] Kostas J., Soria J., Chong M.S., *Particle image velocimetry measurements of a backward-facing step flow.*, Exp Fluids **33**, 838–853, 2002.

[23] Li, Z., Gao, N., Bai, H. *Effect of the periodic perturbations on the wall pressure downstream of a backward facing step.*, International Conference on Fluid Mechanics **25**, 00–00, 2015.

[24] Lumley, J.L., *The structure of inhomogeneous turbulent flows.*, Atmospheric Turbulence and Radio Wave Propagation (A.M. Yaglom and V.I. Takarski, eds.), Moscow: Nauka. **25**, 166–178, 1967.

[25] Ma, X., Karniadakis, G., Park, H., Gharib, M., *DPIV-driven flow simulation: a new computational paradigm.*, Proc. R. Soc. Series A **459**, 547–565, 2003.

[26] NadgeP.M., Govardhan R.N., *High Reynolds number flow over a backward-facing step: structure of the mean separation bubble.*, Exp Fluids **55**, 55–1657, 2014.

[27] Nishri, B., Wygnanski, I., *Effects of periodic excitation on turbulent flow separation from a flap*, AIAA Journal **36**, 547–556, 1998.

[28] Park, H., Cho, J-H., Lee, J., Lee, D-H., Kim, K-H., *Aerodynamic drag reduction of Ahmed model using synthetic jet array.*, Tech. Rep. SAE Technical Paper.

[29] Roos,F.W., Kegelman, J.T. *Control of Coherent Structures in Reattaching Laminar and Turbulent Shear Layers*, AIAA Journal **24**, 1956–1963, 1986.

[30] RoumÃľas, M., GilliÃľron, P., Kourta, A. *Drag reduction by flow separation control on a car after body.*, Int. J. Num. Meth. Fluids **60** (11), 1222–1240, 2009.

[31] Scarano F., Riethmuller M., *Iterative multigrid approach in PIV image processing with discrete window offset.*, Exp Fluids **26**, 513–523, 1999.

[32] Schmidt, H.J., Woszidlo, R., Nayeri, C.N., Paschereit, C.O., *Drag reduction on a rectangular bluff body with base flaps and fluidic oscillators.*, Exp Fluids **56** (7), 1–16, 2015.

[33] Seifert, A., Pack, L.G., *Oscillatory control of separation at high Reynolds numbers*, AIAA Journal **37**, 1062–1071, 1999.

[34] Simpson R.L., *Aspects of turbulent boundary-layer separation.*, Prog. Aerospace Sci **32**, 457–521, 1996.

[35] Spazzini, P.G., Iuso, G., Onorato, M., Zurlo, N., Di Cicca, G. M., *Unsteady behavior of back-facing step flow*, Exp. Fluids **30**, 551–561, 2001.

[36] Wengle, H., Huppertz, A., BÃd'rwolff, G. and Janke, G. *The manipulated transitional backward-facing step flow: an experimental and direct numerical simulation investigation*, European Journal of Mechanics - B/Fluids **20**, 25–46, 2001.

[37] Yoshioka, S., Obi, S., Masuda, S., *Turbulence statistics of periodically perturbed separated flow over a backward-facing step.*, International Journal of Heat and Fluid Flow **22**, 393–401, 2001.

[38] Yoshioka, S., Obi, S., Masuda, S., *Organized vortex motion in periodically perturbed turbulent separated flow over a backward-facing step.*, International Journal of Heat and Fluid Flow **22**, 301–307, 2001.